Drug Deliv. and Transl. Res. (2012) 2:56–64
DOI 10.1007/s13346-011-0056-9

RESEARCH ARTICLE

Fluorescently labeled microbubbles for facilitating translational molecular ultrasound studies

Patrick Koczera · Zhuojun Wu · Stanley Fokong · Benjamin Theek · Lia Appold · Samuel Jorge · Diana Möckel · Zhe Liu · Adelina Curaj · Gert Storm · Marc van Zandvoort · Fabian Kiessling · Twan Lammers

Published online: 20 January 2012

Abstract Microbubbles (MB) are routinely used as contrast agents for functional and molecular ultrasound (US) imaging. For molecular US imaging, MB are functionalized with antibodies or peptides, in order to visualize receptor expression by angiogenic or inflamed endothelium. In general, initial in vitro binding studies with targeted MB are performed using phase contrast microscopy. Difficulties in the identification of MB in standard phase contrast microscopy, however, generally result in high variability, high observer dependency, and low reproducibility. To overcome these shortcomings, we here describe a simple post-loading strategy for labeling polymer-based MB with fluorophores, and we show that the use of rhodamine-loaded MB in combination with fluorescence microscopy substantially reduces the variability and the observer dependency of in vitro binding studies. In addition, we demonstrate that rhodamine-loaded MB can also be used for in vivo and ex vivo experimental setups, e.g., for analyzing MB binding to inflamed carotids using two-photon laser scanning microscopy, and for validating the binding of VEGFR2-targeted MB to tumor endothelium. These findings demonstrate that fluorescently labeled MB substantially facilitate translational molecular US studies, and they suggest that a similar synthetic strategy can be exploited for preparing drug-loaded MB, to enable image-guided, targeted, and triggered drug delivery to tumors and to sites of inflammation.

Keywords Microbubbles · PBCA · Molecular imaging · Ultrasound · Rhodamine · Two-photon microscopy

P. Koczera · S. Fokong · B. Theek · L. Appold · S. Jorge · D. Möckel · Z. Liu · A. Curaj · F. Kiessling · T. Lammers (✉)
Department of Experimental Molecular Imaging,
RWTH Aachen University,
Aachen, Germany
e-mail: tlammers@ukaachen.de

Z. Wu · A. Curaj · M. van Zandvoort
Institute for Molecular Cardiovascular Research,
RWTH Aachen University,
Aachen, Germany

G. Storm · T. Lammers
Department of Targeted Therapeutics, University of Twente,
Enschede, The Netherlands

G. Storm · T. Lammers
MESA+ Institute for Nanotechnology, University of Twente,
Enschede, The Netherlands

Z. Wu · M. van Zandvoort
Department of Biomedical Engineering,
Maastricht University Medical Centre,
Maastricht, The Netherlands

Introduction

Molecular imaging aims to non-invasively visualize processes taking place at the molecular level, such as receptor expression and enzyme activity [1, 2]. Various different diagnostic modalities can be used for molecular imaging, including, e.g., positron emission tomography, magnetic resonance imaging, optical imaging, and ultrasound (US) imaging. Except for magnetic resonance spectroscopy, all molecular images techniques rely on the use of contrast agents. These agents either specifically bind to receptors overexpressed by target cells (thereby accumulating or retaining more signal at the pathological site), or they are specifically cleaved by enzymes (thereby generating signal at the pathological site) [3, 4].

The contrast agents used in molecular US imaging are based on antibody- or peptide-functionalized microbubbles (MB). MB are gas-filled vesicles stabilized by a lipid- or polymer-based shell; the former are generally referred to as soft-shell MB, the latter as hard-shell MB. In spite of the fact that they differ in various aspects, such as in size, stability, biodegradability, circulation time, and acoustic properties, both soft-shell and hard-shell MB are highly suitable contrast agents for molecular US imaging [5, 6].

Because of their size, which is in the range of 1–5 μm, MB remain strictly within the vascular compartment. This is both an advantage and a disadvantage. Concerning the latter, it, on the one hand, limits the use of MB for molecular imaging purposes, as they can only be used for visualizing receptors (over-) expressed by endothelial and by blood cells. Conversely, concerning the former, the fact that MB do not extravasate, means that there will not be any unspecific accumulation at the target site, not even in highly leaky tumors, thereby minimizing the background signal and consequently maximizing the signal-to-noise ratio in molecular US studies.

Several molecular US approaches are currently being considered for clinical translation. These include MB targeted to the vascular endothelial growth factor receptor 2 (VEGFR2), for monitoring tumor angiogenesis in prostate cancer [7–9], and MB targeted to the vascular cell adhesion molecule 1 (VCAM1) and P-selectin, for imaging and staging atherosclerotic plaques [10, 11]. Also RGD-targeted MB, which bind to the angiogenesis-associated integrins $\alpha_v\beta_3$ and $\alpha_v\beta_5$, and ICAM1-antibody-targeted MB, which bind to the inflammation marker intercellular adhesion molecule 1, have been extensively evaluated in recent years, and also these MB seem to hold significant potential for clinical translation [5, 8, 11–14].

The suitability of antibody- or peptide-targeted MB for molecular US imaging is generally initially evaluated in vitro. This can either be done under standard (static) cell culture conditions, or in a flow chamber, to mimic physiological shear stress. In both cases, a layer of endothelial cells is exposed to untargeted MB, to targeted MB, and to targeted MB in the presence of an excess of blocking antibody (usually 10–100 fold; to validate binding specificity). After incubating for 5–30 min, the amount of MB binding to target cells is then visualized and quantified using phase contrast microscopy [7, 9]. As exemplified by the left panels in Fig. 2, however, it is very difficult to unambiguously identify and accurately quantify MB binding using phase contrast microscopy. Consequently, the results obtained in such initial in vitro analyses typically are highly observer-dependent, the variability tends to be high, and the reproducibility tends to be low.

To overcome these shortcomings, and to facilitate translational molecular US studies, we here present a simple post-loading strategy to label polymer-based MB with fluorophores. Using rhodamine as a model compound, we show that fluorophore labeling substantially reduces the variability typically observed in in vitro binding studies, and that it improves the accuracy of blocking experiments. In addition, we show that rhodamine-labeled MB can be used for visualizing and validating in vitro and ex vivo MB binding to angiogenic and inflamed endothelium, using both standard fluorescence microscopy and two-photon microscopy.

Materials and methods

Synthesis of rhodamine-labeled streptavidin-coated PBCA microbubbles

Streptavidin-coated poly(*n*-butyl cyanoacrylate) (PBCA) microbubbles were synthesized as described in [8]. Briefly, monomeric butyl-2-cyanoacrylate (BCA; Sichel Werke GmbH) was added to an acidic aqueous solution of 1% Triton X-100 (Sigma-Aldrich Co.) and stirred vigorously, resulting in a suspension of PBCA MB. Subsequently, the MB were purified and size-isolated by centrifugation as described in [15], to obtain MB with an average size of ~2 μm. Fluorophore labeling was performed by adding 1 mL of a 1.5-mg/mL solution of rhodamine (Acros Organics BVBA) to 10 mL of the purified MB solution (containing 10^9 MB per mL), and the mixture was gently stirred for 10 min. After several flotation steps to remove excess free rhodamine, carboxylate groups were introduced into the shell of the MB by hydrolysis with 0.1 N NaOH. Streptavidin (Chem-Impex International Inc.) was coupled to the generated carboxylate groups via carbodiimide chemistry, using 1-ethyl-3-(3-dimethylaminopropyl) carbodiimide hydrochloride (EDC; Sigma-Aldrich Co.). Three flotation steps were performed to remove excess reactants, and were followed by size and concentration analyses using a Beckmann Coulter Counter (Multisizer 3 Beckmann Coulter Inc.). Rhodamine encapsulation into the shell of the MB was validated using fluorescence microscopy (Axio Imager M2 microscope; Carl Zeiss AG; 400-fold magnification).

Synthesis of antibody-targeted rhodamine-labeled PBCA microbubbles

The rhodamine-labeled streptavidin-coated PBCA MB were targeted against the epidermal growth factor receptor (EGFR; as a model cell surface receptor). This was done by incubating 2 μL of a 1-mg/mL solution of a biotinylated mouse monoclonal antibody directed against human EGFR (Abcam) with 1 mL of MB solution (at a concentration of 10^7 per mL) for 10 min. The solution was washed by flotation to remove unbound antibodies. MB targeted against

VEGFR2, which were used in the in vivo experiment, were prepared similarly, i.e., by mixing 50 μL containing 10^7 rhodamine-labeled and streptavidin-coated MB with 1.5 μl of a 0.5-mg/mL solution of biotinylated rat monoclonal antibody directed against murine VEGFR2 (BioLegend Inc.). In both cases, antibody-free rhodamine-labeled streptavidin-coated PBCA MB were used as controls.

Cell culture

A431 epidermoid carcinoma cells were obtained from ATCC. Cells (10^5) were seeded on glass coverslips in six-well plates (Becton, Dickinson and Company). They were cultured in 2 mL of RPMI medium, supplemented with 100 μL/mL fetal bovine serum, 100 U/mL penicillin, and 100 μg/mL streptomycin (all from Life Technologies Corporation) until reaching a confluency of ~50%. Human umbilical vein endothelial cells were also obtained from ATCC, and were seeded on 35 mm collagen-coated Petri dishes (Becton, Dickinson and Company), at a density of 10^5. They were cultured in 2 ml of ECGM supplemented with Endothelial Cell Growth Supplement Mix (PromoCell GmbH) and 100 μg/mL gentamycin (Life Technologies Corporation) reaching ~80% confluency. For the in vivo experiment, CT26 murine colon carcinoma cells (ATCC) were cultured in DMEM, supplemented with 100 μL/mL fetal bovine serum, 100 U/mL penicillin, and 100 μg/mL streptomycin until reaching ~90% confluency.

In vitro binding studies

Prior to the in vitro binding studies, medium was removed from the culture dishes and replaced by Dulbecco's Phosphate-Buffered Saline (DPBS; Life Technologies Corporation). Subsequently, the DPBS was removed and 1 ml DPBS containing 10^7 EGFR-targeted MB and 5 μg Hoechst 33258 (Sigma-Aldrich Co.; for nuclear staining) was added. As controls, 10^7 non-targeted MB or 10^7 EGFR-targeted MB in the presence of a 10-fold excess (i.e., 20 μL; for competition purposes) of free anti-EGFR antibody was added. The cells were incubated with the different MB formulations for 15 min. To facilitate the contact between the (otherwise floating) MB and the cells, the coverslips were placed upside down, and the MB were introduced underneath. After incubation, the cells were washed three times with DPBS. The coverslips were then mounted using Mowiol 4-88 (Carl Roth GmbH & Co. KG) and MB binding was analyzed using an Axio Imager M2 microscope (Carl Zeiss AG). For the analysis of specific MB binding, several random pictures were taken, both in phase contrast and in fluorescence mode, of three coverslips per experimental condition. The Hoechst-stained nuclei and the rhodamine-labeled MB were analyzed upon excitation at 359 and 558 nm, and emission at 461 and 583 nm, respectively, at a magnification of ×400.

Ten independent observers counted the number of cells and of attached MB per field of view (FOV) in five different images, initially in phase contrast mode, and then in fluorescence mode. For evaluating binding specificity, 10 images were analyzed per condition (i.e., non-targeted, EGFR-targeted, and EGFR-targeted plus excess free antibody). Counting was again initially performed in phase contrast mode and then in fluorescence mode.

HUVEC were stimulated to express inflammatory markers using recombinant human TNFα (ProSpec-Tany TechnoGene Ltd.). This was done for 4 h, prior to the binding study, at a TNFα concentration of 40 ng/mL. One hour prior to the binding study, cell membranes were stained with Alexa Fluor 488-conjugated wheat germ agglutinin (WGA-AF488; at a dilution of 1:500) and nuclei were stained with SYTO41 (at a dilution of 1:1000; both markers were obtained from Life Technologies Corporation). The 35-mm Petri dishes were mounted on a customized parallel-wall flow chamber. Subsequently, 300 μl DPBS containing 10^7 ICAM1-targeted or non-targeted control MB were injected into the tube connecting both ends of the flow chamber. A peristaltic pump (Gilson, Inc.) was used to circulate the MB for 10 min, at a flow rate of 0.25 mL/min. Then, the loop was opened, unbound MB were washed out, and HUVEC were washed with 2.5 mL of DPBS. Images were acquired using an Olympus FV1000MPE multiphoton microscopy system, equipped with a Mai Tai DeepSee femtosecond pulsed Ti:Sapphire laser. The objective lens used was an ×60 water dipping, while the excitation wavelength was chosen to be 800 nm. Three photomultiplier tubes were used to detect the fluorescence signals, and filters were adjusted to the corresponding emission spectra, i.e., 465–480 nm for SYTO41, 490–560 nm for WGA-AF488, and 560–600 nm for rhodamine-labeled MB. Z-directional image series (z-stacks) were recorded for 3D image reconstruction. All image-processing analyses were performed using Image-Pro 3D analyzer 7.0 software (Media Cybernetics, Inc).

In vivo binding studies

After inoculating 10^6 CT26 cells subcutaneously into the flank of an 8-week-old female mouse, the tumor was allowed to grow for 10 days, until reaching a size of ~6×6 mm. Molecular US imaging was performed using the Vevo 2100 imaging system with a MS250 transducer (VisualSonics Inc.), at a frequency of 21 MHz and at a power of 4%. Then, 10^7 VEGFR2-targeted MB were injected i.v. via the tail vein, in a total injection volume of ~50 μl. Seven minutes after i.v. injection, two image sequences (consisting of several frames, before and after destructive pulses) were performed, in non-linear contrast mode. Images were analyzed using the Vevo2100 Imaging Software, Version 1.2.1. Two minutes

prior to sacrificing the animal, 75 μl of fluorescein-labeled lectin (Ricinus Communis Agglutinin I; 5 mg/mL; Vector Laboratories, Inc.) were injected i.v. Subsequently, the mouse was perfused intracardially under deep anesthesia with 50 mL of heparinized DPBS and sacrificed, followed by tumor excision. The excised tumor was mounted in OCT compound (Sakura Finetek Europe B. V.), frozen at −80°C and cut into 8-μm thick slices using a CM3050S cryostat (Leica Microsystems GmbH). Finally, fluorescence microscopy was performed at a ×400 magnification to visualize the perfusion of blood vessels (using fluorescein-labeled lectin) and the binding of VEGFR2-targeted rhodamine-labeled MB to angiogenic tumor endothelium.

Statistical analysis

All results are presented as average±standard deviation. Depending on the experimental setup, statistical significance was analyzed either using the unpaired Student's *t* test (binding specificity), or using the *F* test (variance). $P<0.05$ was considered to represent statistical significance.

Results and discussion

Synthesis and characterization of rhodamine-labeled PBCA microbubbles

The size and size distribution of the rhodamine-labeled MB is shown in Fig. 1a. This size distribution, which is in the order of 1.5–2 μm, has been reported to be optimal for in vivo US imaging because it reduces the dose of polymer (PBCA) injected without a substantial loss in contrast enhancement [15]. Given the fact that hard-shell MB have a much thicker shell than soft-shell MB, (i.e., ~50 vs. ~3–5 nm; [15, 16]), it is possible to encapsulate small molecules like rhodamine in the shell of polymer-based MB. Fluorescence microscopy (Fig. 1b) confirmed the encapsulation of rhodamine in the MB shell. The post-loading method used for rhodamine encapsulation provides a versatile tool for loading MB with low molecular weight compounds. Besides for fluorophore labeling, this strategy could also be used for entrapping drug molecules into the shell of polymer-based MB, to thereby enable image-guided, targeted, and triggered drug delivery to tumors and to sites of inflammation. However, to provide proof-of-principle for such purposes, additional analyses addressing, e.g., encapsulation efficiency, the stability of drug loading, and the release of the encapsulated agents upon the application of destructive US pulses have to be performed.

Fluorophore labeling facilitates in vitro MB binding experiments

Subsequently, EGFR-binding antibodies were conjugated to the shell of the rhodamine-loaded MB (via biotin-streptavidin coupling), and their ability to bind to EGRF-overexpressing A431 cells was visualized using both phase contrast and fluorescence microscopy. As exemplified by Fig. 2, fluorescence labeling not only substantially facilitated the quantification of the number of bound MB, but also the accurate determination of the number of cells per field of view (FOV). In standard phase contrast microscopy, the number of cells per FOV can be estimated based on the borders of the cells or on nuclear structures, but this method clearly is fairly inaccurate and observer-dependent (Fig. 2a–b). Conversely, upon labeling cellular nuclei with Hoechst, the number of cells per FOV could be determined with high accuracy, with

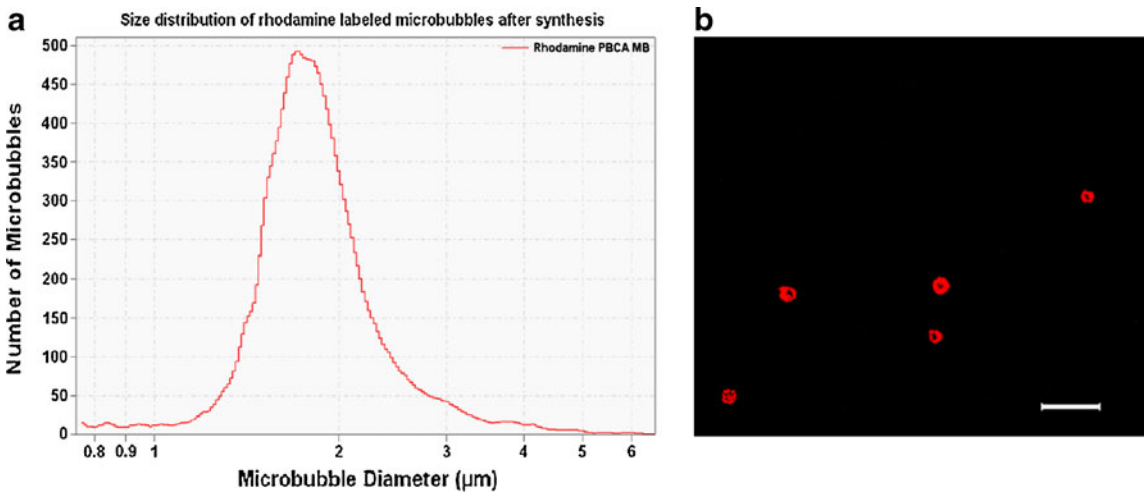

Fig. 1 Rhodamine-labeled poly(*n*-butyl cyanoacrylate) microbubbles. **a** Size and size distribution of PBCA MB post-loaded with rhodamine, evaluated using Coulter Counter analysis. **b** The encapsulation of rhodamine into the MB shell and the relatively narrow size distribution of the MB was confirmed using fluorescence microscopy. *Bar*=10 μm

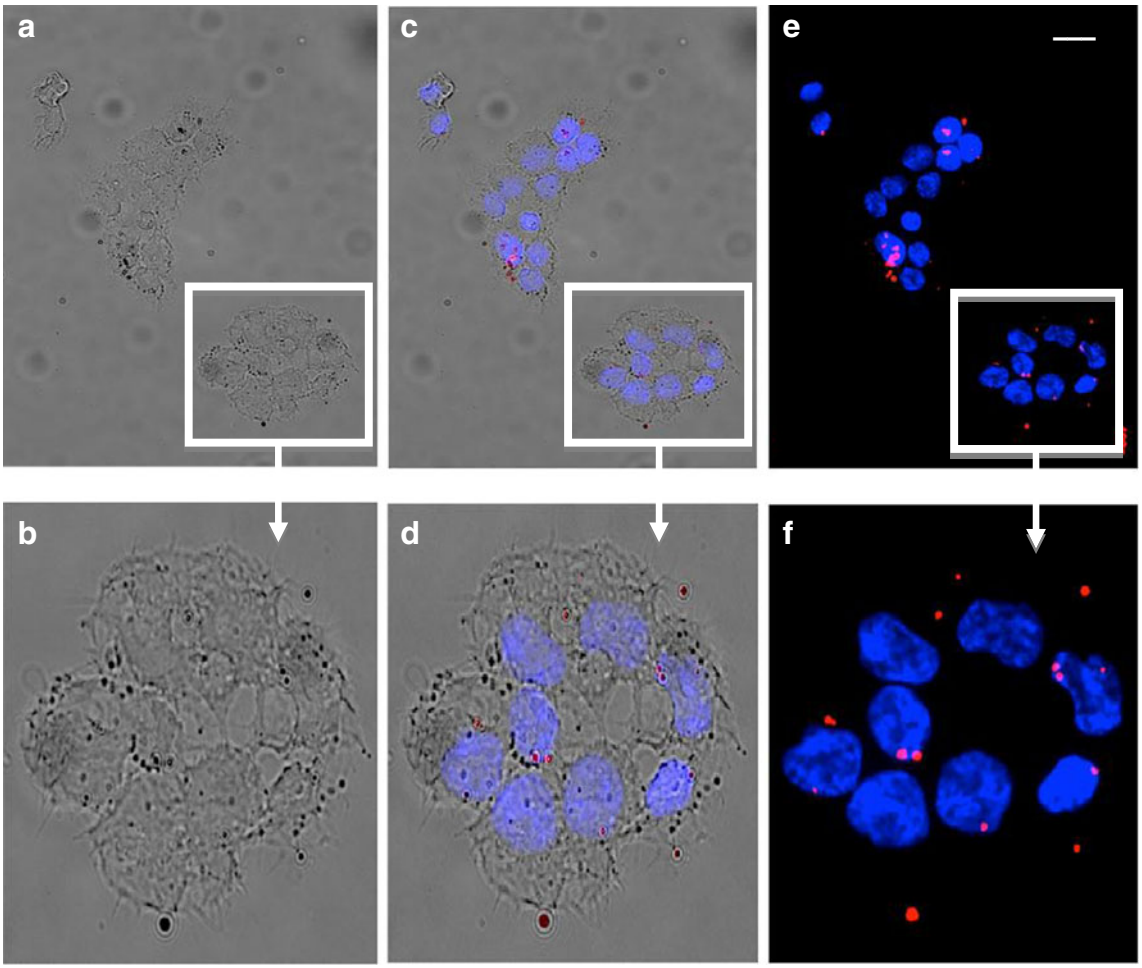

Fig. 2 Facilitating in vitro binding studies using fluorescently labeled MB. A431 cells were incubated for 15 min with rhodamine-loaded EGFR-antibody-targeted MB, and MB binding was visualized using standard phase contrast microscopy (**a**–**b**) and fluorescence microscopy (**e**–**f**). It can be clearly seen that fluorescence labeling facilitates the in vitro distinction between MB and MB-like structures (cf. *left vs. right panels*). Rhodamine-loaded MB are shown in *red*, Hoechst-labeled nuclei in *blue*. *Bar*=20 μm

high reproducibility, and with very low interindividual variability (Fig. 2e–f). This is quantitatively confirmed in Fig. 3c and in Table 1, showing that the variance in the number of cells per FOV was significantly lower when 10 different observers determined the number of cells in five different FOV using fluorescence microscopy (VA=0–0.03) as compared to phase contrast microscopy (VA=0.06–0.16).

Analogously, as shown in Fig. 3d and in Table 1, also the interindividual variability in the number of bound MB per FOV could be significantly reduced upon using rhodamine-labeled MB in combination with fluorescence microscopy. Given the general difficulty of accurately and reproducibly identifying MB in phase contrast images (Fig. 2a–b), the difference in the number of bound MB per FOV was much larger in this case (Fig. 3d). For phase contrast-based analyses, the variance ranged from 0.36 to 1.42, as compared to only 0.07–0.28 for fluorescence microscopy (Table 1).

As a result of the reduced variance in both the number of cells and the number of bound MB, also the variance in the number of bound MB per cell was found to be decreased in case of rhodamine-labeled MB and fluorescence microscopy (Fig. 3e). This is very important, as the number of bound MB per cell is generally used as the main parameter to evaluate the in vitro specificity of MB binding. As shown in Table 1, the variance in this case ranged from 0.33 to 1.74 for phase contrast microscopy, as compared to only 0.08–0.28 for fluorescence microscopy. Moreover, as demonstrated in Fig. 3e, no clear tendency towards an increased number of bound MB per cell per FOV could be observed in the five images in Fig. 3a when using phase contrast microscopy: the average number appeared to be lowest for image 2, and highest for image 3. Conversely, when analyzing these images using fluorescence microscopy (Fig. 3b), a gradual increase in the number of bound MB per cell could be observed, with the lowest value for image 1, and the highest value for image 5. These findings convincingly demonstrate that

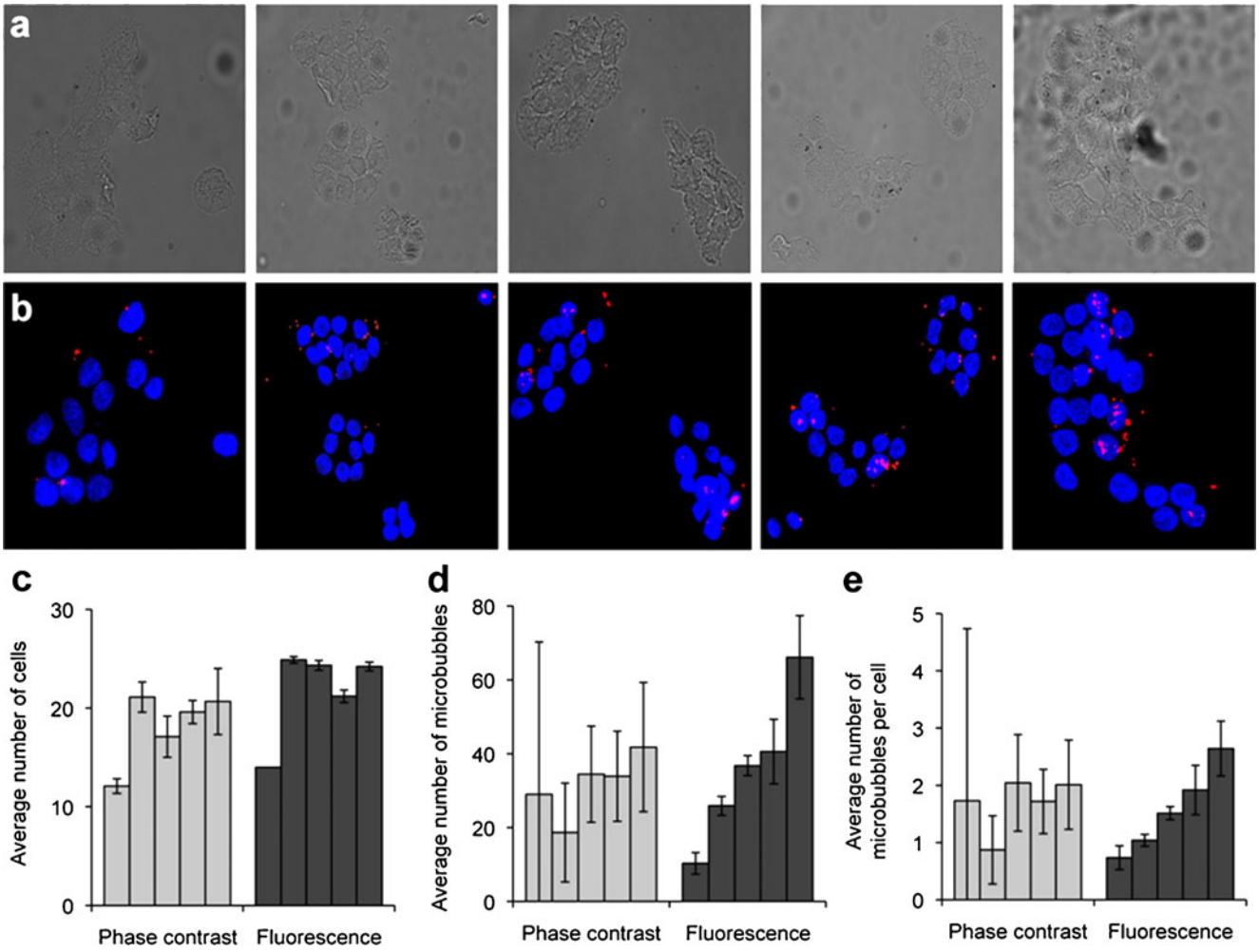

Fig. 3 Reducing the variability of in vitro binding studies using fluorescently labeled MB. A431 cells were incubated for 15 min with rhodamine-loaded EGFR-antibody-targeted MB, and the number of cells, of bound MB, and of bound MB per cell was quantified. **a**–**b** Five different FOV were analyzed by 10 different observers, using both standard phase contrast microscopy (**a**) and fluorescence microscopy (**b**). **c**–**e** Quantitative analysis of the average number of cells per FOV (**c**), of the average number of bound MB per FOV (**d**), and of the average number of bound MB per cell (**e**), upon phase contrast and fluorescence microscopy. Values represent average±standard deviation (n=10). It can be clearly seen that combining rhodamine-labeled MB with fluorescence microscopy significantly reduces the interindividual variability of in vitro binding experiments

Table 1 Variance analysis for the in vitro binding studies performed using phase contrast and fluorescence microscopy with rhodamine-loaded EGFR-antibody-targeted MB. The values are based on the images and results presented in Fig. 3

Image		Number of cells		Number of MB		Number of MB/cell	
		Phase contrast	Fluorescence	Phase contrast	Fluorescence	Phase contrast	Fluorescence
1	Variance	0.06	0	1.42	0.28	1.74	0.28
	P value	N.A.		<0.0001		<0.0001	
2	Variance	0.07	0.01	0.72	0.10	0.68	0.10
	P value	0.0001		<0.00001		<0.0001	
3	Variance	0.12	0.02	0.38	0.07	0.41	0.08
	P value	0.0001		0.0001		<0.0001	
4	Variance	0.06	0.03	0.36	0.22	0.33	0.23
	P value	0.08		0.34		0.45	
5	Variance	0.16	0.02	0.42	0.17	0.39	0.18
	P value	<0.0001		0.27		0.19	

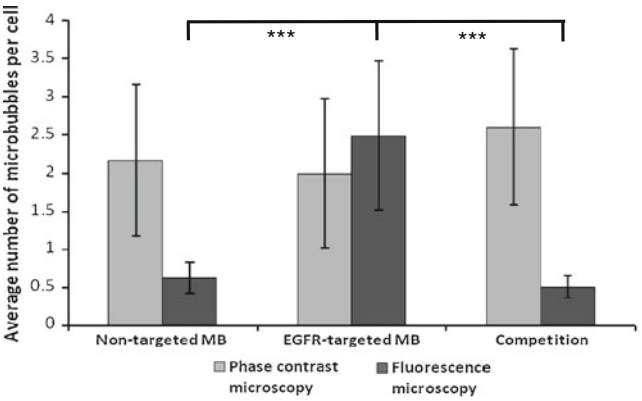

Fig. 4 Improving the accuracy of in vitro MB binding and blocking experiments. A431 cells were incubated for 15 min with fluorescently labeled non-targeted MB, with EGFR-antibody-targeted MB, and with EGFR-antibody-targeted MB in the presence of excess free EGFR-antibody (competition). Ten different FOV were analyzed per experimental condition, using both standard phase contrast microscopy (*light gray*) and fluorescence microscopy (*dark gray*). Values are presented as average number of bound MB per cell±standard deviation per FOV (n=10). As can be clearly seen, the combination of rhodamine-labeled MB with fluorescence microscopy substantially improves the accuracy of in vitro MB binding and blocking experiments. Asterisks indicate $p<0.0001$

labeling MB with fluorophores reduces the variability and increases the accuracy and the reproducibility of in vitro MB binding experiments.

Fluorophore labeling improves quantitative in vitro analyses on MB binding specificity

To validate the above observations, we subsequently performed an experiment in which EGFR-targeted MB were compared to non-targeted MB and to EGFR-targeted MB under competition conditions. As shown in Fig. 4, when using phase contrast microscopy, no significant difference was found when 10 randomly chosen FOV were analyzed. When analyzing the same FOV using fluorescence microscopy, however, a clear and highly significant difference could be observed between targeted and non-targeted MB ($p<0.0001$). Analogously, also upon blocking specific MB binding using a 10-fold excess of free EGFR-antibody, a highly significant difference was observed upon using fluorescence microscopy ($p<0.0001$). These results show that the simple post-loading of fluorescent dyes into MB substantially improves the information obtained in in vitro binding and blocking experiments, that it renders statistically highly superior results, and that it therefore holds significant potential for implementation in future translational molecular US studies.

Visualizing and validating MB binding to the angiogenic endothelium

Besides for facilitating in vitro binding studies, fluorescently labeled MB can also be used for several other purposes. Some

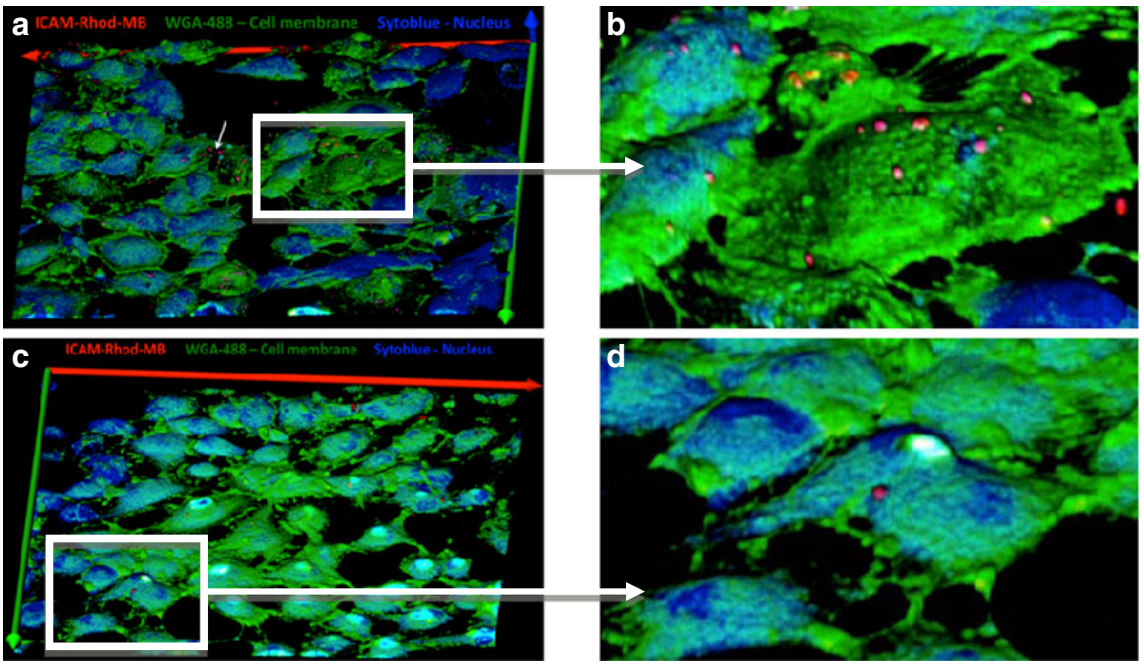

Fig. 5 Visualizing and quantifying the binding of fluorescently labeled ICAM1-antibody-targeted MB to inflamed endothelial cells using two-photon laser scanning microscopy. Four hours prior to MB incubation, HUVEC were either stimulated with TNFα (to mimic inflammatory conditions and to upregulate the expression of ICAM1 (**a**–**b**) or sham-treated (**c**–**d**). Then, the cells were exposed to rhodamine-loaded ICAM1-antibody-targeted MB (*red*) for 10 min, and MB binding was visualized using TPLSM. Nuclei were counterstained with SYTO41 (*blue*), cell membranes were stained with WGA-AF488 (*green*). Strong and specific MB binding to TNFα-stimulated HUVEC (**a**–**b**), but not to unstimulated HUVEC (**c**–**d**), could be clearly visualized

examples of this are provided in Figs. 5 and 6. In Fig. 5, the binding of ICAM1-targeted MB to stimulated (A–B) and unstimulated (C–D) human umbilical vein endothelial cells (HUVEC) is shown, as visualized using two-photon laser scanning microscopy (TPLSM). In these images, rhodamine-labeled MB are depicted in red, cell membranes in green (WGA-AF488), and nuclei in blue (SYTO41). Similar studies can also be performed ex vivo, using customized flow chambers and excised blood vessels [17, 18]. In such setups, viable plaque-containing blood vessels from animals suffering from atherosclerosis can be visualized three dimensionally [19], and the binding of different types of antibody-targeted and fluorescently labeled MB to the inflamed vascular wall and/or to plaque surfaces can be analyzed at high resolution using TPLSM (Wu et al., manuscript in preparation).

Another potentially interesting application of fluorescently labeled MB relates to the ex vivo validation of in vivo MB binding to angiogenic endothelium. Figure 6 provides an example of this, demonstrating that VEGFR2-targeted MB bind with high specificity to tumor blood vessels in a subcutaneous CT26 tumor. Panel A shows the tumor before MB administration, and panel B shows the same tumor 7 min after the i.v. injection of the MB. It should be noted that at this time point, hardly any MB are present in systemic circulation anymore, since their half-life time is ~1 min [20]. Consequently, the bright spots observed in the tumor at this time point can be attributed exclusively to bound MB (Fig. 6c). To quantify the amount of MB bound to the tumor vasculature, several high mechanical index destructive pulses are then applied, and the signals before

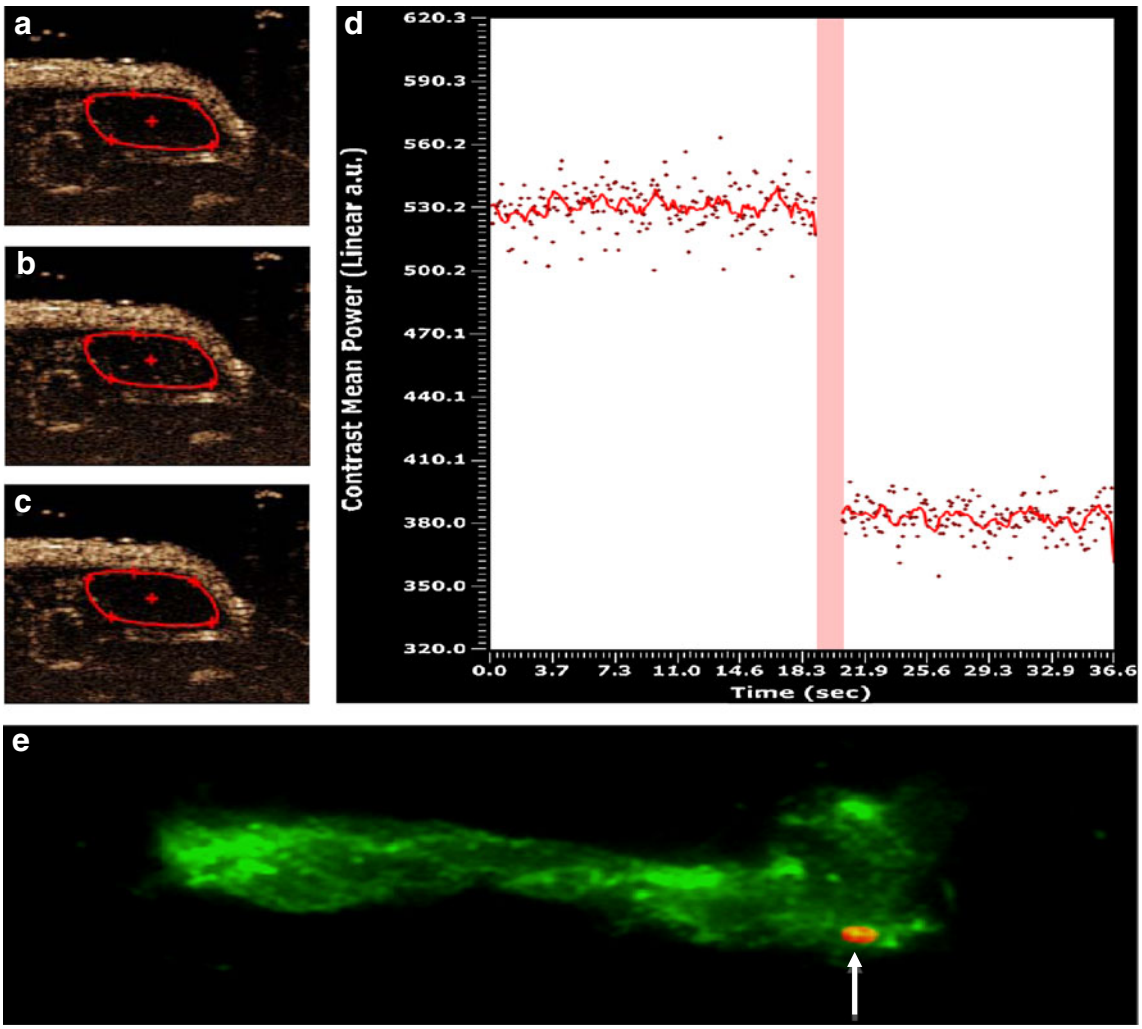

Fig. 6 In vivo molecular US imaging and ex vivo fluorescence microscopy validation of MB binding to angiogenic tumor endothelium. **a**–**c** US imaging of a CT26 tumor prior to MB administration (**a**), 7 min after the i.v. injection of VEGFR2-antibody-targeted MB (**b**), and immediately after the application of a high mechanical index destructive US pulse (**c**). **d** Quantification of the loss of tumor-specific US signal, generated using MB, following the application of the destructive pulse, demonstrating highly specific MB binding to the tumor vasculature. **e** Ex vivo fluorescence microscopy-based validation of specific MB binding (in *red*; see *arrow*) to angiogenic tumor endothelium (counterstained using fluorescein-labeled lectin; in *green*)

and after destruction are analyzed. As exemplified by Fig. 6d, using this type of molecular US imaging, a high level of VEGFR2-specific MB binding to angiogenic tumor endothelium could be observed in this particular CT26 tumor. To validate MB binding to the tumor vasculature, the animal was perfused with fluorescein-labeled lectin (which stains blood vessels) prior to tumor excision, and the specific binding of rhodamine-labeled and VEGFR2-targeted MB to angiogenic endothelium (in tumor areas not exposed to destructive pulses) could be nicely visualized using fluorescence microscopy (Fig. 6e). In a similarly sized CT26 tumor treated with non-targeted MB, no adherent MB were observed, neither in in vivo molecular US experiments, nor in ex vivo fluorescence microscopy validation experiments.

Together, our findings convincingly demonstrate that the simple post-loading of polymer-based hard-shell MB with fluorophores substantially facilitates translational molecular US studies, enabling not only less observer-dependent and more accurate in vitro binding experiments, but also in vitro and ex vivo validation experiments, in which standard fluorescence microscopy and TPLSM are used to confirm specific MB binding to angiogenic and inflamed endothelium. Moreover, our findings indicate that besides model fluorophores, likely also low molecular weight drugs can be encapsulated relatively efficiently within the shell of polymer-based MB, to thereby enable image-guided, targeted and triggered drug delivery to tumors and to sites of inflammation.

Acknowledgments The authors kindly acknowledge financial support by the DFG and by HighTech.NRW, as well as technical assistance from Anne Rix, Susanne Arns and Marek Weiler.

References

1. Weissleder R, Mahmood U. Molecular imaging. Radiology. 2001;219(2):316–33.
2. Massoud TF, Gambhir SS. Molecular imaging in living subjects: seeing fundamental biological processes in a new light. Genes Dev. 2003;17(5):545–80.
3. Rudin M, Weissleder R. Molecular imaging in drug discovery and development. Nat Rev Drug Discov. 2003;2(2):123–31.
4. Herschman HR. Molecular imaging: looking at problems, seeing solutions. Science. 2003;302(5645):605–8.
5. Kiessling F, Huppert J, Palmowski M. Functional and molecular ultrasound imaging: concepts and contrast agents. Curr Med Chem. 2009;16(5):627–42.
6. Kiessling F, Gaetjens J, Palmowski M. Application of molecular ultrasound for imaging integrin expression. Theranostics. 2011;1:127–34.
7. Willmann JK, Paulmurugan R, Chen K, Gheysens O, Rodriguez-Porcel M, Lutz AM, et al. US imaging of tumor angiogenesis with microbubbles targeted to vascular endothelial growth factor receptor type 2 in mice. Radiology. 2008;246(2):508–18.
8. Palmowski M, Huppert J, Ladewig G, Hauff P, Reinhardt M, Mueller MM, et al. Molecular profiling of angiogenesis with targeted ultrasound imaging: early assessment of antiangiogenic therapy effects. Mol Cancer Ther. 2008;7(1):101–9.
9. Tardy I, Pochon S, Theraulaz M, Emmel P, Passantino L, Tranquart F, et al. Ultrasound molecular imaging of VEGFR2 in a rat prostate tumor model using BR55. Invest Radiol. 2010;45(10):573–8.
10. Kaufmann BA, Carr CL, Belcik JT, Xie A, Yue Q, Chadderdon S, et al. Molecular imaging of the initial inflammatory response in atherosclerosis: implications for early detection of disease. Arterioscler Thromb Vasc Biol. 2010;30(1):54–9.
11. Lindner JR. Contrast ultrasound molecular imaging of inflammation in cardiovascular disease. Cardiovasc Res. 2009;84(2):182–9.
12. Hamilton AJ, Huang SL, Warnick D, Rabbat M, Kane B, Nagaraj A, et al. Intravascular ultrasound molecular imaging of atheroma components in vivo. J Am Coll Cardiol. 2004;43(3):453–60.
13. Klibanov AL. Ultrasound molecular imaging with targeted microbubble contrast agents. J Nucl Cardiol. 2007;14(6):876–84.
14. Palmowski M, Peschke P, Huppert J, Hauff P, Reinhardt M, Maurer M, et al. Molecular ultrasound imaging of early vascular response in prostate tumors irradiated with carbon ions. Neoplasia. 2009;11(9):856–63.
15. Fokong S, Siepmann M, Liu Z, Schmitz G, Kiessling F, Gätjens J. Advanced characterization and refinement of poly N-butyl cyanoacrylate microbubbles for ultrasound imaging. Ultrasound Med Biol. 2011;37(10):1622–34.
16. Hoff L, Sontum PC, Hovem JM. Oscillations of polymeric microbubbles: effect of the encapsulating shell. J Acoust Soc Am. 2000;107(4):2272–80.
17. Megens RT, Reitsma S, Schiffers PH, Hilgers RH, De Mey JG, Slaaf DW, et al. Two-photon microscopy of vital murine elastic and muscular arteries. Combined structural and functional imaging with subcellular resolution. J Vasc Res. 2007;44(2):87–98.
18. Megens RT, Oude Egbrink MG, Cleutjens JP, Kuijpers MJ, Schiffers PH, Merkx M, et al. Imaging collagen in intact viable healthy and atherosclerotic arteries using fluorescently labeled CNA35 and two-photon laser scanning microscopy. Mol Imaging. 2007;6(4):247–60.
19. Megens RT, oude Egbrink MG, Merkx M, Slaaf DW, van Zandvoort MA. Two-photon microscopy on vital carotid arteries: imaging the relationship between collagen and inflammatory cells in atherosclerotic plaques. J Biomed Opt. 2008;13(4):044022.
20. Palmowski M, Morgenstern B, Hauff P, Reinhardt M, Huppert J, Maurer M, et al. Pharmacodynamics of streptavidin-coated cyanoacrylate microbubbles designed for molecular ultrasound imaging. Invest Radiol. 2008;43(3):162–9.